Remote Sensing of Cloud Properties using Ground-based Measurements of Zenith Radiance

J. Christine Chiu[1], Alexander Marshak[2], Yuri Knyazikhin[3], Warren J. Wiscombe[2]
Howard W. Barker[4], James C. Barnard[5], Yi Luo[6]

[1] Joint Center for Earth Systems Technology, University of Maryland Baltimore County, Baltimore, MD
[2] Climate and Radiation Branch, NASA/Goddard Space Flight Center, Greenbelt, MD
[3] Department of Geography, Boston University, Boston. MA
[4] Meteorological Service of Canada, Downsview, Ontario, Canada
[5] Pacific Northwest National Laboratory, Richland, WA
[6] Noetix Research Inc., Ottawa, Ontario, Canada

Abstract

An extensive verification of cloud property retrievals has been conducted for two algorithms using zenith radiances measured by the Atmospheric Radiation Measurement (ARM) Program ground-based passive two-channel (673 and 870 nm) Narrow Field-Of-View Radiometer. The underlying principle of these algorithms is that clouds have nearly identical optical properties at these wavelengths, but corresponding spectral surface reflectances (for vegetated surfaces) differ significantly. The first algorithm, the RED vs. NIR, works for a fully three-dimensional cloud situation. It retrieves not only cloud optical depth, but also an effective radiative cloud fraction. Importantly, due to one-second time resolution of radiance measurements, we are able, for the first time, to capture detailed changes in cloud structure at the natural time scale of cloud evolution. The cloud optical depths τ retrieved by this algorithm are comparable to those inferred from both downward fluxes in overcast situations and microwave brightness temperatures for broken clouds. Moreover, it can retrieve τ for thin patchy clouds, where flux and microwave observations fail to detect them. The second algorithm, referred to as COUPLED, couples zenith radiances with simultaneous fluxes to infer τ. In general, the COUPLED and RED vs. NIR algorithms retrieve consistent values of τ. However, the COUPLED algorithm is more sensitive to the accuracies of measured radiance, flux, and surface reflectance than the RED vs. NIR algorithm. This is especially true for thick overcast clouds where it may substantially overestimate τ.

1. Introduction

Cloud optical depth τ is an important cloud property and is vital for any cloud-radiation parameterization. To estimate τ from measurements, the atmospheric science community has widely used ground-based flux measurements from both broadband [*Leontieva and Stamnes*, 1994; *Boers*, 1997] and narrowband [*Min and Harrison*, 1996; *Leontieva and Stamnes*, 1996] radiometers. This type of technique is, however, limited to overcast conditions and at best, gives "effective" values of τ instead of "local" values [*Ricchiazzi et al.*, 1995; *Dong et al.*, 1997].

Unlike flux instruments, narrow field-of-view (NFOV) radiometers that measure zenith radiance have the potential to provide less *effective*, more *local* estimates of τ. There are, however, two major problems with inferring τ from monochromatic zenith radiance. First, it is known from 1D plane-parallel radiative transfer theory that the relationship between τ and zenith radiance is a double-valued function. This is demonstrated, using the Discrete-Ordinate-method (DISORT) [*Stamnes et al.*, 1988], in Fig. 1: it is clearly impossible, in general, to unambiguously retrieve τ from just a one-channel NFOV radiometer. Second, the histogram of actual observations (solid line in Fig. 1) from ARM's one-channel NFOV radiometer reveals that due to 3D effects, some radiances exceed those permitted by 1D models. This results in τ being irretrievable for some zenith radiances.

Marshak et al. [2000] and *Barker and Marshak* [2001] proposed different approaches to reduce the retrieval ambiguity of radiance-based algorithms. *Marshak et al.* [2000] estimated τ from two-channel radiance [673 nm (RED) and 870 nm (NIR)] measurements. The underlying principle of their algorithm is that these two channels have similar cloud properties but strong spectral contrast in vegetated surface reflectance. By analogy with the normalized difference vegetation index (NDVI) [*Tucker*, 1979], they introduced a normalized difference cloud index (NDCI) as the ratio of the difference to the sum of normalized zenith radiances at the two channels, in an attempt to isolate information pertaining to τ. However, it was found that τ could vary considerably while NDCI remained unchanged.

Instead of using a single index, *Marshak et al.*, [2004] created look-up tables and utilized directly radiance observations on the RED vs. NIR plane. Figure 2 shows a schematic illustration of this retrieval approach. Since most vegetated surface are dark at RED wavelengths and bright at NIR wavelengths, points above the diagonal correspond to cloudy situations due to surface-cloud interactions, while points below the diagonal correspond to clear sky. Since the surface is dark in the RED region, having the same RED radiances in points A and B indicates that they have the same values of τ. However, they have different radiances in the NIR region. Clearly, more surface-cloud interactions occur and more photons reach the ground for point B. This indicates that point B corresponds to a smaller cloud fraction than point A. Therefore, from the RED vs. NIR plane, not only can τ be retrieved, but so too can an "effective" cloud fraction. Note that points A and C have the same NDCI (lying on the same line and having the

same slope), but apparently they correspond to different values of τ and effective cloud fractions. This algorithm is referred to hereinafter as the "RED vs. NIR" algorithm.

The concept of the algorithm proposed by *Barker and Marshak* [2001], and studied theoretically by *Knyazikhin et al.* [2005], also relies on this strong spectral difference of the surface-cloud interactions. They coupled zenith *radiances* along with time series of *flux* measurements to infer τ. Henceforth, this is called the "COUPLED" algorithm. Their method has been tested for model-simulated clouds and associated radiation fields. To assess the performance of this algorithm in more realistic conditions, *Barker et al.* [2004] have evaluated τ retrievals with cloud model-generated data that release the frozen turbulence assumption originally used in *Barker and Marshak* [2001].

The objectives of this paper is to assess the RED vs. NIR and the COUPLED algorithms using ARM observations, and to illustrate cloud evolution and advection with high temporal resolution retrievals. The ARM program deployed a surface-based two-channel Narrow Field-of-View Radiometer (2NFOV) at the Southern Great Plains (SGP) central facility in September 2004. This radiometer measures downwelling zenith radiance at 673 and 870 nm, has a 5.7° field of view, and one-second temporal resolution. With 1 s resolution data, we are able, for the first time, to capture detailed changes in cloud structure.

In an attempt to deduce whether 2NFOV measurements contain biases, section 2 compares 2NFOV measurements with those from CIMEL observations of the Aerosol Robotic Network (AERONET) [*Holben et al.*, 1998]. If necessary, 2NFOV data are calibrated toward CIMEL measurements. In section 3, we briefly review the methodologies of the RED vs. NIR and the COUPLED algorithms. Sensitivity tests of algorithms to sources of uncertainty are included in section 4, as well as special remarks regarding the COUPLED algorithm. To put the performance of these algorithms into context, our retrievals are compared with those estimated from other radiometers, such as the ARM Multi-Filter Rotating Shadowband Radiometer (MFRSR) and Microwave Radiometer (MWR). Section 5 presents retrieval results of all algorithms for various situations including near-homogeneous clouds, broken clouds, and problematic cases that algorithms have difficulties dealing with. Summary and discussions are given in section 6.

2. Comparisons with the CIMEL

Since the accuracy of AERONET's CIMEL measurements meets a high standard [*Holben et al.*, 1998], the ARM 2NFOV radiances are compared to the CIMEL in order to quantify any biases in the 2NFOV data. The CIMEL sunphotometer is a ground-based radiometer used for aerosol studies that looks directly toward the Sun,has a 1.2° field of view, and four filters at 440, 670, 870, and 1020 nm. When the Sun is blocked by clouds, CIMEL operates in "cloud mode" where it takes 10 measurements of zenith radiance with a 9-second temporal resolution [*Marshak et al.*, 2004].

Figure 3 shows ARM 2NFOV radiances vs. CIMEL measurements at the SGP site for the period Nov. 3 to 30, 2004; sample size is ~3000 data points. This plot reveals that these two data sets correlate well, but the ARM 2NFOV radiometer tends to underestimate zenith radiance at 673 and 870 nm by about 20% and 10%, respectively. Based on regression analyses, 2NFOV zenith radiances were adjusted using

$$\begin{aligned} I_{RED,adj} &= \left(I_{RED,obs} + 0.000587\right)/0.82 \\ I_{NIR,adj} &= \left(I_{NIR,obs} + 0.000400\right)/0.92 \end{aligned} \tag{1}$$

where the subscript *obs* represents original measured zenith radiances, and *adj* is for radiances after the adjustment. This adjustment was absolutely necessary in order to make a meaningful comparison between our retrievals and those estimated from other instruments. Retrieval results shown in this paper are based on the adjusted radiances.

3. Algorithms

3.1 The RED vs. NIR algorithm

For plane-parallel clouds over a Lambertian surface, any ground-based measurement of radiance I can be given as [*Liou*, 2002, pp. 365-366],

$$I = I_0 + \frac{\rho I_s T_0}{1 - \rho R} \tag{2}$$

where I_0 is radiation calculated for a non-reflecting surface, and the second term on the right side is radiation due to interactions between clouds and the surface. The surface-cloud interactions depend on albedo ρ of the underlying Lambertian surface, radiation I_s from an isotropic source located at the surface, transmittance T_0 for a nonreflecting surface, and spherical albedo of clouds R given uniform, isotropic upwelling illumination from below. Approximating T_0 with

$$T_0 = 1 - A_c + A_c \cdot T_{0,pp} \tag{3}$$

where A_c is cloud fraction and $T_{0,pp}$ is transmittance for non-reflecting surface in a plane-parallel assumption, we can rewrite (3) as a function of cloud optical depth τ and A_c as:

$$\begin{aligned} I_1(\tau, A_c) &= I_{0,1}(\tau) + \frac{\rho_1 I_{s,1}(\tau) \cdot \left[1 - A_c + A_c T_{0,pp,1}(\tau)\right]}{1 - \rho_1 R_1(\tau)} \\ I_2(\tau, A_c) &= I_{0,2}(\tau) + \frac{\rho_2 I_{s,2}(\tau) \cdot \left[1 - A_c + A_c T_{0,pp,2}(\tau)\right]}{1 - \rho_2 R_2(\tau)}, \end{aligned} \tag{4}$$

where subscripts 1 and 2 represent wavelengths λ_1 and λ_2, respectively. We assume that the dependency on A_c comes only from (3). Note that this A_c is not a *real* cloud fraction,

but rather a "radiatively effective" value that forces 3D measurements fit into 1D plane-parallel radiative transfer calculations. Detailed explanations and discussions can be found in *Marshak et al.* [2004].

As expected from (4), surface albedo has a strong impact on radiances in a forward problem, and thus on retrieved τ and A_c in the inverse problem. In this paper, we used surface reflectivity parameters provided by the Canada Centre for Remote Sensing. Their products were optimally derived from a number of satellites [*Luo et al.*, 2005]. We further used DISORT to calculate $I(\tau, A_c)$ for both wavelengths (as in (4)) over a reasonable range of cloud optical depths and cloud fractions. By comparing measurements with 2D lookup tables, it is possible to infer both cloud optical depth and effective cloud fraction simultaneously. For λ_1 and λ_2 we use the RED and NIR channels, respectively.

3.2 The COUPLED algorithm

This section outlines a number of key steps of the COUPLED algorithm that combines zenith radiance with flux measurements to infer cloud optical depths [*Barker and Marshak*, 2001; *Knyazikhin et al.*, 2005]. For plane-parallel clouds over a horizontally homogeneous Lambertian surface with a surface albedo ρ, transmittance T can be rewritten as [*Petty*, 2004, pp. 413]

$$T = \frac{T_0}{1 - \rho R} \tag{5}$$

Combining (2) and (5) gives

$$\begin{aligned} I_1 &= I_{0,1} + \rho_1 T_1 I_{s,1}; \\ I_2 &= I_{0,2} + \rho_2 T_2 I_{s,2}, \end{aligned} \tag{6}$$

where subscripts 1 and 2 again represent wavelengths of λ_1 and λ_2, respectively. If two wavelengths with identical cloud properties are selected, then $I_{0,1} = I_{0,2}$ and $I_{s,1} = I_{s,2} = I_s$, and so

$$I_2 - I_1 = \left(\rho_2 T_2 - \rho_1 T_1\right) \cdot I_s(\tau). \tag{7}$$

For a homogeneous Lambertian surface, transmittance T relates to upwelling flux F_{up} as

$$F_{up} = \rho T F_0, \tag{8}$$

where F_0 is solar irradiance at the TOA at a given wavelength. Let us define $F^{\uparrow}$ as the upward flux normalized by F_0. For simplicity, also normalize I_1, I_2, and I_s, so that (7) can be rewritten as

$$I_2 - I_1 = \left(F_2^{\uparrow} - F_1^{\uparrow}\right) \cdot I_s(\tau), \tag{9}$$

or

$$I_s(\tau) = \frac{I_2 - I_1}{F_2^{\uparrow} - F_1^{\uparrow}}, \tag{10}$$

where all quantities are assumed dimensionless hereinafter.

How can (10) be justified for application to inhomogeneous clouds? For horizontally inhomogeneous clouds, (9) can be written as [*Knyazikhin et al.*, 2005]

$$I_2(x) - I_1(x) = \int_{x' \in S} \left[F_2^{\uparrow}(x') - F_1^{\uparrow}(x') \right] \cdot J(x,x')dx', \tag{11}$$

where S is the underlying surface; $F_1^{\uparrow}(x')$ and $F_2^{\uparrow}(x')$ are downward fluxes at location x' on the surface at wavelength 1 and 2, respectively; $J(x,x')$ is the wavelength independent probability that a photon from an isotropic source $1/\pi$ located at x' arrives at location x after the surface-cloud interaction. *Knyazikhin et al.* [2005] defined a bottom-of-atmosphere reflectance at location x as

$$r_\lambda(x) = \frac{\int_{x' \in S} F_\lambda^{\uparrow}(x') J(x,x')dx'}{F_\lambda^{\uparrow}(x')}, \tag{12}$$

where the numerator describes the surface-cloud interactions when clouds are illuminated from below by horizontally inhomogeneous isotropic sources $F_\lambda^{\uparrow}(x')$. While the downwelling flux, and thus the upwelling flux $F_\lambda^{\uparrow}(x')$, can vary significantly, the ratio (12) will not necessarily have a large variation. As shown by them, $r_\lambda(x)$ approximates the maximum eigenvalue of the linear operator defined by the numerator of (12). Thus, it can be assumed to be wavelength independent, i.e., $r_\lambda(x) = r(x)$. Substituting (12) into (11) gives

$$r(x) \approx \frac{I_2(x) - I_1(x)}{F_2^{\uparrow}(x) - F_1^{\uparrow}(x)}. \tag{13}$$

Note that a simple combination of wavelength dependent radiances and fluxes in (13) eliminates wavelength dependency and relates only to cloud structure above x. Comparing with the ratio in (10) for a plane-parallel geometry, we can write

$$I_s(x,\tau) \approx \frac{I_2(x) - I_1(x)}{F_2^{\uparrow}(x) - F_1^{\uparrow}(x)} \tag{14}$$

which justifies the use of (10) for horizontally inhomogeneous clouds.

How can $F_\lambda^{\uparrow}$ be measured? Since MFRSR provides downwelling fluxes only, (14) cannot be applied directly for cloud optical depth retrieval. Models of the two-point $J(x,x')$ correlation function are needed to relate downwelling and upwelling fluxes in 3D

environment. For a plane-parallel geometry with a homogeneous Lambertian surface they are related simply as $F_\lambda^\uparrow(x) = \rho_\lambda F_\lambda^\downarrow(x)$. Since in the general case such models of J are not yet available, we approximate $F_\lambda^\uparrow(x)$ using a simple technique proposed by Barker and Marshak [2001]. This technique integrates measured downwelling fluxes over a given time-interval using weighting functions that account for cloud base altitude and cloud advection rate. Once $F_\lambda^\uparrow(x)$ is calculated, I_s is derived from (14) and used in lookup tables to infer τ.

4. Remarks of the COUPLED algorithm

4.1 Effects of assumption $I_{0,1} = I_{0,2}$

As mentioned in section 3.2, the COUPLED algorithm is based on an assumption that downward radiance for a non-reflecting surface (i.e., I_0) in these two channels is similar. Effects of the assumption $I_{0,1} = I_{0,2}$ on retrieved τ are discussed in this section. To quantify the error due to this assumption, two sets of synthetic data were tested. The first data set was generated using the Henyey-Greenstein phase function for cloud droplets with asymmetry factors of 0.856 and 0.851 that correspond to λ_1 (RED) and λ_2 (NIR) wavelengths, respectively. The second data set was based on Mie phase functions assuming an effective radius of 8 μm; they have asymmetry factors equal to those just mentioned.

In the general case of $I_{0,1} \neq I_{0,2}$, it follows from (6) that

$$I_s = \frac{I_2 - I_1}{\rho_2 T_2 - \rho_1 T_1} + \frac{I_{0,1} - I_{0,2}}{\rho_2 T_2 - \rho_1 T_1}, \tag{15}$$

where the second term on the right hand side accounts for $I_{0,1} \neq I_{0,2}$. The COUPLED algorithm works well only if this term is negligible compared to the first one on the right hand side, and thus no substantial retrieval errors are introduced assuming $I_{0,1} = I_{0,2}$.

The percentage of the second term relative to I_s is plotted in Fig. 4. Based on the data generated from the Henyey-Greenstein phase function, for a significant surface reflectance contrast, the assumption of $I_{0,1} = I_{0,2}$ introduces errors that are < 10% (Fig. 4a). This error goes up significantly with a decreasing contrast in surface albedo (Fig. 4b), though the error is reduced with a decreasing cloud fraction (not shown). When the Mie phase functions were used, the error increased (Fig. 4c and d). For a small contrast in surface albedo (e.g., $\rho_1 = 0.1$, $\rho_2 = 0.3$), the assumption $I_{0,1} = I_{0,2}$ contributes more than 25% error in I_s for overcast, thick clouds (Fig. 4d). This error becomes even greater when the solar zenith angle (SZA) is large. Note that since $I_{0,1} > I_{0,2}$ for all τ except very small ones, the second term in (15) is *positive*. Thus, the assumption of $I_{0,1} = I_{0,2}$ introduces a bias that always *underestimates* τ.

An apparently possible solution to eliminate this bias for the COUPLED method is to retrieve τ directly from lookup tables using the ratio $(I_2 - I_1)/(\rho_2 T_2 - \rho_1 T_1)$ instead of I_s. However, this ratio is not a monotonic function of τ. The lack of one-to-one relationship starts at different values of τ depending upon the surface albedo contrast, cloud fraction and SZA. In general, this function looses its uniqueness at smaller optical depth when the surface albedo contrast is small, the sky is overcast, and SZA is large.

4.2 Effects of measurement uncertainties

This section aims to evaluate the sensitivity of the COUPLED algorithm to the uncertainty: 1) in measurements of both radiance and flux; and 2) in surface albedo. Unlike the previous subsection, we assume that $I_{0,1} = I_{0,2}$ to completely isolate the effects of measurement uncertainties on retrievals. This sensitivity test is conducted using synthetic measurements that are generated from the Henyey-Greenstein phase function with an asymmetry factor of 0.856 for both channels.

Figure 5a shows the ranges of retrieved cloud optical depths that respond to 1% uncertainty in both radiances and fluxes with a SZA of 60°. When the sky is overcast (A_c = 1) and the surface albedo contrast is significant (e.g., $\rho_1 = 0.0$, $\rho_2 = 0.5$), 1% measurement uncertainty produces roughly a 20–50% variation in retrievals. Variations of retrievals are dramatically magnified when the surface albedo contrast becomes smaller (e.g., $\rho_1 = 0.1$, $\rho_2 = 0.3$). However, for broken clouds (e.g., $A_c = 0.5$), fluctuations in retrieved cloud optical depth are reduced since more radiation reaches the surface thus enhancing surface-cloud interactions.

It is important to point out that the uncertainty in measurements leads to a much larger degree of overestimation in retrieval than that of underestimation. Let us take the case of $\rho_1 = 0.1$, $\rho_2 = 0.3$, and $A_c = 1$ as an example. At the true optical depth of 30 in Fig. 5a, 1% measurement uncertainty introduces an underestimation in cloud optical depth by 30% (retrieved $\tau = 20$), but also might cause an overestimation in retrievals by almost 100% ($\tau \approx 60$). In this example, we assume only 1% measurement uncertainty. However, according to the ARM instrument handbook, flux measurement uncertainties can be as large as 5%. The achievement of 1% accuracy in radiance is also quite challenging. Therefore, for the COUPLED algorithm, measurement uncertainties can significantly *overestimate* cloud optical depths when $\tau > 30$.

The sensitivity of the COUPLED algorithm to the uncertainty in surface albedo is illustrated in Fig. 5b. We assume $\rho_1 = 0.1$ and $\rho_2 = 0.3$ with 10% and 5% uncertainty, respectively, which are comparable to the accuracies of current available surface reflectance products in RED and NIR channels from satellite measurements [Schaaf et al., 2002]. As expected, retrieval uncertainty for thicker clouds is substantially larger than for thinner ones. In short, the COUPLED algorithm is expected to work better for (*i*) optically thinner, (*ii*) broken clouds above surfaces with (*iii*) a large contrast between RED and NIR reflectance. If even one of these three conditions is violated, resulting

retrievals can be less reliable. This may indicate that the retrieval of τ is an ill-posed problem.

4.3 Joint effects

We have demonstrated that the assumption of $I_{o,1} = I_{o,2}$ in the COUPLED method introduces a bias that always underestimates τ, and measurement uncertainties significantly overestimate τ. These biases might be reduced or even cancelled out to yield reasonable retrievals in some circumstances. However, in many cases the bias is not eliminated completely and thus highly unstable overestimations appear in retrievals, especially for overcast-sky situations.

We have also emphasized the importance of surface reflectance contrast in the RED and NIR channels for the COUPLED algorithm. Note that not only spectral difference in surface reflectance matters here, but also their absolute values. By ratioing the reflectance difference between these two channels by their sum, the normalized difference vegetation index (NDVI) presents useful information on such a surface reflectance contrast. Larger NDVI values indicate more significant spectral contrasts in surface reflectance. For instances, for $\rho_1 = 0.0$ and $\rho_2 = 0.5$, NDVI = (0.5-0.0)/(0.5+0.0) = 1. This index reduces to 0.5 for $\rho_1 = 0.1$ and $\rho_2 = 0.3$. Figure 6 shows NDVI values for the ARM SGP site during 2004 as estimated from the Moderate Resolution Imaging Spectroradiometer (MODIS). During the observation period, NDVI values were between 0.35 and 0.4, which is not the best condition for our retrieval purpose. Nevertheless, evaluations for this period still help us to better understand the performance of all algorithms, and to identify problems that need to be addressed.

To conclude for the COUPLED algorithm:

(i) The more inhomogeneous clouds are, the more stable are the retrieved cloud optical depths. The algorithm works best when $A_c << 1$.

(ii) The less optically thick clouds are, the more reliable are the retrieved optical depths. Based on the analyses in this section, the algorithm works best when $\tau \leq 30$.

(iii) The larger the spectral contrasts in surface reflectance are, the more reliable and stable are the retrievals. The algorithm works best when NDVI > ~0.4.

5. Results

In this section we describe the performance of the RED vs. NIR and the COUPLED algorithms in various cloud situations, along with two other benchmark algorithms. The first benchmark algorithm is based on ARM MFRSR measurements [*Min and Harrison*, 1996]. The MFRSR provides spectral measurements of total solar flux at 415, 500, 615, 673, 870, and 940 nm every 20 seconds. We infer cloud optical depths from observed atmospheric transmittances derived from downward fluxes.

The second benchmark algorithm estimates τ from microwave-retrieved liquid water path (LWP). The ARM microwave radiometer (MWR) measures brightness temperatures at 23.8 and 31.4 GHz every 20 seconds, and has a 5.9° of field-of-view that is comparable to the 2NFOV radiometer (5.7°). We obtained retrieved LWP from the ARM standard product. Since an 8 μm effective radius of cloud droplets (typical for the ARM Oklahoma ARM site) was assumed to construct lookup tables for the RED vs. NIR, and the COUPLED algorithms, we applied the same effective radius in the conversion of LWP to τ.

Three of these algorithms retrieve cloud optical depths only; the RED vs. NIR algorithm additionally gives an effective cloud fraction. For illustration, we add sky images that were taken every 30 seconds by the ARM Total Sky Imager (TSI). If available, we also show retrievals from the AERONET CIMEL measurements that are taken in "cloud mode".

5.1 Overcast

Figure 7 demonstrates retrievals for a visually overcast case where clouds are thick but not necessarily homogeneous. In general, retrieved τ from the RED vs. NIR algorithm are in a good agreement with those from MWR and CIMEL. As expected, retrievals from MFRSR show much less fluctuations due to the use of hemispherical total downward fluxes.

As expected from the sensitivity analysis, for thick clouds and overcast sky, retrievals from the COUPLED algorithm show significant fluctuations. In addition to large solar zenith angles (70–75°), the contrast in surface reflectance was also low with NDVI = 0.35 (see Fig. 6). As a result of all four factors (thick clouds, overcast sky, large SZA, and small NDVI), the COUPLED algorithm is unstable and substantially overestimates τ. Interestingly enough, the performance of the COUPLED algorithm improves when the cloud inhomogeneity increases, as the following case shows.

Figure 8 shows another overcast case in which clouds show considerable inhomogeneity. The corresponding distribution of radiance measurements on our 2D lookup table is also plotted in Fig. 9, showing that most observations fall into our lookup table. Data points with a larger radiance at 673 nm than 870 nm correspond to clear-sky situations.

In this case, there is great similarity among all retrievals. However, because of one sec resolution the RED vs. NIR algorithm captures detailed cloud evolutions and advections. For example, the TSI image shows a clear-sky gap at 17.2 UTC (Fig. 8b). This gap corresponds to a small retrieved τ and zero effective cloud fraction. Two and half minutes later, a darker cloud in the left-bottom quadrant of the center shows up and passes toward the right-upper quadrant (Fig. 8c and d) through the 2NFOV field of view. This cloud is much darker compared to surrounding clouds, and so results in a peak in the

time series of retrieved τ. This cloud was also caught by the COUPLED algorithm. The microwave radiometer seems to detect it, but with a much smaller sensitivity.

5.2 Broken clouds

Figure 10 demonstrates retrievals of a patchy cloud for 21.6 to 21.7 UTC, Sep. 29, 2004. Some small cumulus clouds surrounded the outer ring of the center of the TSI images for most of the period. During 21.62 to 21.65 UTC, a patchy cloud passed by and was detected by both the RED vs. NIR and the COUPLED algorithms as a cloud. Obviously, MFRSR measurements are not sensitive enough to detect this cloud. Note that since for small τ contours with various effective cloud fractions are very close to each other in our lookup tables (as shown in Fig. 9), an effective cloud fraction cannot be retrieved accurately here (thus not shown).

Another broken cloud case when clouds moved very rapidly is illustrated in Fig. 11 between 17.6 and 17.7 UTC on Oct. 28. These significant cloud transitions are revealed in the retrievals of cloud optical properties from the RED vs. NIR algorithm. However up to now, no comparable observations or retrievals are available to validate our high temporal resolution retrievals. We can only intercompare these retrievals with a coarse resolution.

The microwave radiometer has the most similar field-of-view to the 2NFOV radiometer, and thus we expected substantial similarity in retrievals from these two instruments. When relatively thick clouds are in the FOV, cloud optical depths inferred from the MWR and 2NFOV are very close (as shown in Fig. 11b and c). However, we found that in some cases with thin clouds in the FOV (e.g., Fig. 11d), the RED vs. NIR algorithm yielded small cloud optical depths, while the MWR was not able to catch them due to a low temporal resolution.

Retrievals from the COUPLED algorithm demonstrate the influences from both the radiance and flux measurements, as expected. Thus, most retrievals are somewhere between the values inferred from the RED vs. NIR algorithm and the MFRSR. Note that a number of retrievals from the RED vs. NIR algorithm suddenly jumped from small values (about 3) to very large values (above 15). We found these situations occurred when cumulus clouds just passed by and the instrument's field-of-view was not fully filled by clouds. These problematic situations will be discussed in the next section.

5.3 Clear-sky contamination

A segment of Oct. 28, 2004 is selected (Fig. 12) to illustrate a potential problem of the "narrow" field-of-view, which is not narrow enough in cloud property retrievals. For instance, retrievals show that there are some unreasonably large (up to 40) cloud optical depths around 17.53 UTC. Looking at the center of the TSI image, the left-upper quadrant had some small cumulus clouds at this time, but the other three quadrants were clear. This cloud moved out 30 seconds later as shown in the next TSI snapshot. It is evident that there is no cloud thick enough to produce such large optical depths.

This retrieval error is attributed to the clear sky parts of the field-of-view. The situation with partially cloudy and partially clear within the FOV leads to small radiances at both channels (as shown in Fig. 13a). The RED vs. NIR algorithm fails since it cannot differentiate this situation from optically thick clouds that also produce small radiances (Fig. 13b). This problem, referred to here as the "clear-sky contamination problem", occurs on many other days. Therefore, the FOV of the ARM 2NFOV radiometer has recently been reduced to 1.2° to lower the probabilities of clear-sky contaminations, and will be further tested in the ARM field campaign.

5.4 Cloud edge

Finally, Fig. 14 illustrates how the RED vs. NIR algorithm fails to estimate cloud optical depths in a 1-minute time period (21.37 to 21.39 UTC). For this period, the MFRSR is also unable to retrieve information regarding these clouds, but the COUPLED algorithm yields reasonable retrievals. Data points in this period have very large radiances at both channels. From the TSI images, one can see that the edges of clouds are around the center and are illuminated directly by the sun. This situation causes a substantial amount of photons to scatter into the field-of-view (as schematically illustrated in Fig. 15), and results in large radiances that are far away from the area that 2D lookup tables can cover. Based on current data, the occurrence of this situation is less than 10%, and is more frequent when the SZA is large. We expect to review this problem when we have new measurements using a 1.2° field-of-view.

6. Summary and discussions

An algorithm, called the RED vs. NIR algorithm (*Marshak et al.*, 2004), has been developed to retrieve cloud optical depth in a fully 3D cloud situation using the new ARM ground-based passive two-channel narrow-field-of-view (2NFOV) measurements. The essence of this algorithm is to infer cloud optical properties using strong contrast in the surface-cloud interactions between the 673 (RED) and 870 nm (NIR) channels. In addition to cloud optical depth, it also provides an *effective* cloud fraction.

Results demonstrate that this algorithm is able to capture local, rapid evolutions and advections of clouds. Note that there is no comparable measurement available yet to validate our one-second resolution retrievals. However, we found that retrievals from the RED vs. NIR algorithm showed consistent cloud optical depths with MFRSR for overcast cases and with MWR for inhomogeneous thicker clouds.

We have also evaluated the performance of the COUPLED algorithm (*Barker and Marshak*, 2001) that infers cloud optical depths from both radiance and flux measurements. This algorithm generally yields similar cloud optical depths to those from the RED vs. NIR algorithm. However, it is more sensitive to uncertainties in radiance, flux, and surface albedo than the RED vs. NIR algorithm. In addition, the COUPLED algorithm becomes unstable for overcast cases with small spectral contrast in surface

reflectance. In these cases, it often substantially overestimates retrieved cloud optical depths. Its retrievals are more reliable for thinner and broken clouds.

The RED vs. NIR algorithm wrongly retrieves large cloud optical depths when the measurement FOV is not fully filled with clouds. Therefore, the FOV of the 2NFOV radiometer has been decreased to 1.2° recently, which should help to achieve less interference from clear-sky and cloud edge. The ARM program has deployed this newest 2NFOV radiometer in a field campaign at Point Reyes, California during June–September 2005. This site is ideal for the RED vs. NIR and the COUPLED algorithms since there is a much larger spectral contrast in surface reflectance than the ARM SGP site (see Fig. 6). Since a substantial amount of data will be collected, we plan to systematically evaluate the RED vs. NIR algorithm with other benchmark algorithms. Furthermore, the ARM has started building a new six-channel NFOV radiometer, having exactly the same wavelengths as the MFRSR. We plan to extend the principle of the RED vs. NIR algorithm to other surface types, and explore suitable channels to infer cloud optical properties.

Acknowledgments

This research was supported by the Office of Science (*BER*, U.S. Department of Energy, Interagency Agreement No. DE-AI02-95ER61961 and DE-FG02-05ER63955.) as part of the ARM program.

References

Barker, H. W., and A. Marshak (2001), Inferring optical depth of broken clouds above green vegetation using surface solar radiometric measurements, *J. Atmos. Sci.*, 58, 2989-3006.

Barker, H. W., C. F. Pavloski, M. Ovtchinnikov, and E. E. Clothiaux (2004), Assessing a cloud optical depth retrieval algorithm with model-generated data and the frozen turbulence assumption, *J. Atmos. Sci.*, 61, 2951-2956.

Boers, R. (1997), Simultaneous retrievals of cloud optical depth and droplet concentration from solar irradiance and microwave liquid, *J. Geophys. Res.*, 102, 29 881–2989.

Dong, X., T. P. Ackerman, E. E. Clothiaux, P. Pilewskie, and Y. Han (1997), Microphysical and radiative properties of boundary layer stratiform clouds deduced from ground-based measurements, *J. Geophys. Res.*, 102, 23829-23843.

Holben B. N., T. F. Eck, I. Slutsker, D. Tanre, J. P. Buis, A. Setzer, E. Vermote, J. A. Reagan, Y. J. Kaufman, T. Nakajima, F. Lavenu, I. Jankowiak, and A. Smirnov (1998), AERONET - A federated instrument network and data archive for aerosol characterization, *Remote Sens. Environ.*, 66, 1–16.

Knyzaikhin, Y., A. Marshak, and R. B. Myneni (2005), 3D Radiative transfer in vegetation canopies and cloud-vegetation interaction, in *Three-Dimensional Radiative Transfer in Cloudy Atmospheres*, edited by A. Marshak and A. B. Davis, pp. 623-658, Springer-Verlag, New York.

Leontieva, E., and K. Stamnes (1994), Estimations of cloud optical thickness from ground-based measurements of incoming solar radiation in the Arctic, *J. Climate*, 7, 566–578.

Leontieva, E., and K. Stamnes (1996), Remote sensing of cloud optical properties from ground-based measurements of transmittance: a feasibility case, *J. Appl. Meteor.*, 35, 2012–2022.

Liou, K. N. (Ed.) (2002), *An Introduction to Atmospheric Radiation*, 2nd ed., 583pp., Academic Press, California.

Luo, Y., A. P. Trishchenko, R. Latifovic, and Z. Li (2005), Surface bidirectional reflectance and albedo properties derived using a land over-based approach with Moderate Resolution Imaging Spectroradiometer observations, *J. Geophys. Res.*, 110, D01106, doi:10.1029/2004JD004741.

Marshak, A., Y. Knyazikhin, A. B. Davis, W. J. Wiscombe, and P. Pilewskie (2000), Cloud-vegetation interaction: Use of normalized difference cloud index for estimation of cloud optical thickness, *Geophys. Res. Lett.*, 27, 1695-1698.

Marshak, A., Y. Knyazikhin, K. D. Evans, and W. J. Wiscombe (2004), The "RED versus NIR" plane to retrieve broken-cloud optical depth from ground-based measurements, Cloud-vegetation interaction: Use of normalized difference cloud index for estimation of cloud optical thickness, *J. Atmos. Sci.*, 61, 1911-1925.

Min, Q. L., and L. C. Harrison (1996), Cloud properties derived from surface MFRSR measurements and comparison with GOES results at the ARM SGP site, *Geophys. Res. Lett.*, 23, 1641–1644.

Petty, G. W. (Ed.) (2004), *A First Course in Atmospheric Radiation*, 444 pp., Sundog, Wisconsin.

Ricchiazzi, P., C. Gautier, and D. Lubin (1995), Cloud scattering optical depth and local surface albedo in the Antarctic - simultaneous retrieval Using ground-based radiometry, *J. Geophys. Res.*, 100, 21091-21104.

Schaaf, C. B., and Coauthors (2002), First operational BRDF, albedo nadir reflectance products from MODIS, *Remote Sens. Environ.*, 83, 135-148.

Stamnes, K., S.–C. Tsay, W. J. Wiscombe and K. Jayaweera (1988), Numerically stable algorithm for discrete-ordinate-method radiative transfer in multiple scattering and emitting layered media, *Appl. Opt.*, 27, 2502–2512.

Tucker, C. J. (1979), Red and photographic infrared linear combination for monitoring vegetation, *Remote Sens. Environ.*, 8, 127-150.

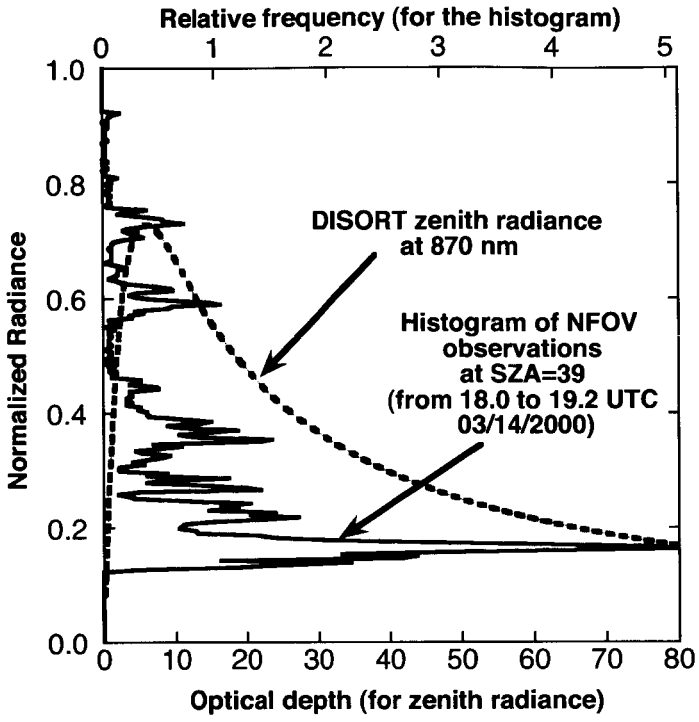

Fig. 1 Downward 870 nm radiances vs. cloud optical depth (lower x-axis) calculated by DISORT with a surface albedo of 0.271. Co-plotted solid curve is a histogram of the ARM one-channel NFOV radiances (870 nm) from 18 to 19.2 UTC, March 14, 2000, using the upper x-axis.

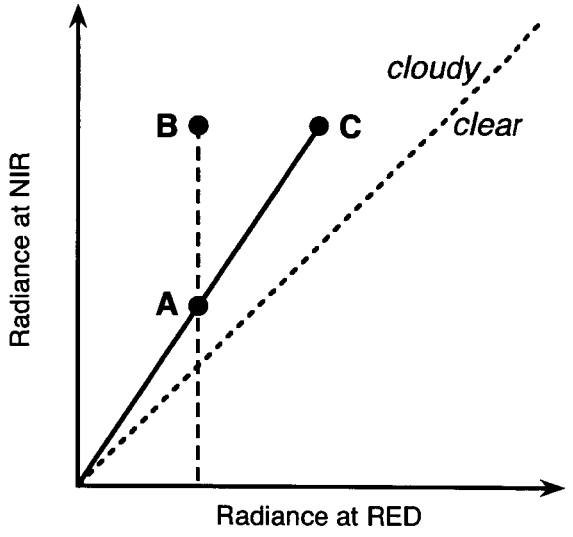

Fig. 2 A schematic illustration of the RED vs. NIR algorithm.

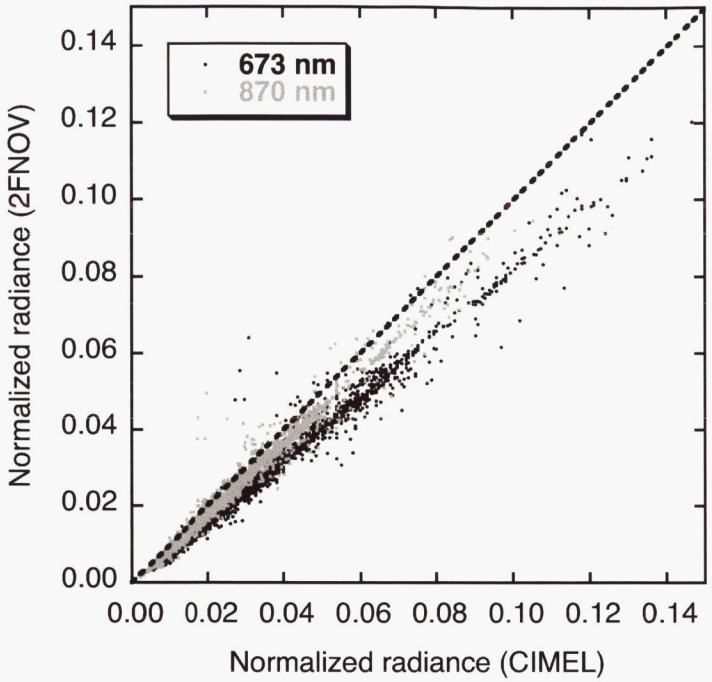

Fig. 3 Scatter-plot of ARM two-channel NFOV measurements vs. CIMEL at channels 673 and 870 nm. Data were collected at the ARM SGP CART site during Nov. 03 to 30, 2004.

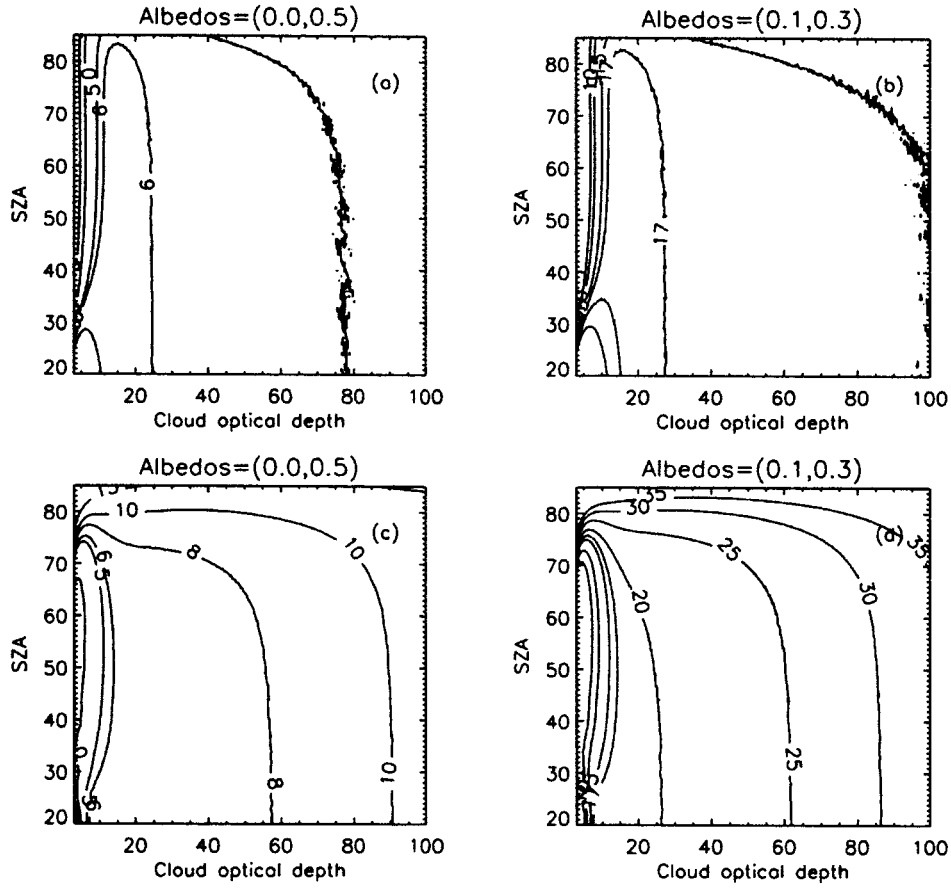

Fig. 4 Contours of error percentages due to the assumption of $I_{o,1} \sim I_{o,2}$ in the COUPLED algorithm when $A_c = 1$. The upper panel is based on the Henyey-Greenstein phase function for (a) $(\rho_1, \rho_2) = (0.0, 0.5)$; and (b) $(\rho_1, \rho_2) = (0.1, 0.3)$. (c) and (d) are the same as (a) and (b), respectively, but based on Mie phase functions.

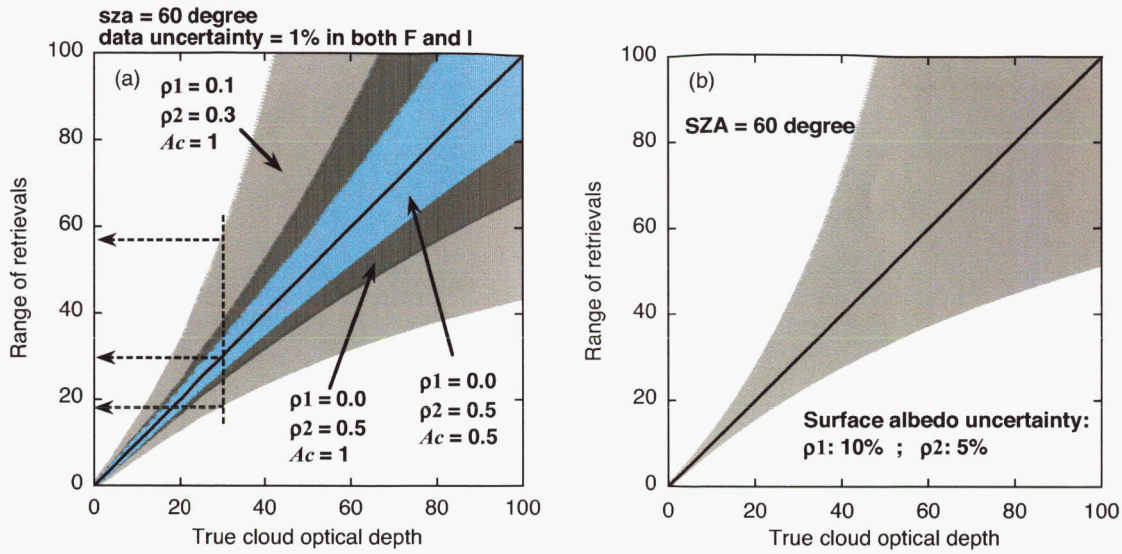

Fig. 5 (a) Fluctuations of cloud optical depth retrievals vs. true value using synthetic data with 1% uncertainty in both radiances and fluxes. Note that the histogram of retrievals is skewed to larger cloud optical depths, i.e., a positive skewness (not shown). Data were generated using the Henyey-Greenstein phase function with an asymmetry factor of 0.856 for both channels. Shades from outside to inner represent the ranges of retrieved cloud optical depths, based on $\rho_1 = 0.1$, $\rho_2 = 0.3$, $A_c = 1$; $\rho_1 = 0.0$, $\rho_2 = 0.5$, $A_c = 1$; and $\rho_1 = 0.0$, $\rho_2 = 0.5$, $A_c = 0.5$, respectively. (b) Same as (a), but for $\rho_1 = 0.1 \pm 10\%$, $\rho_2 = 0.3 \pm 5\%$, $A_c = 1$.

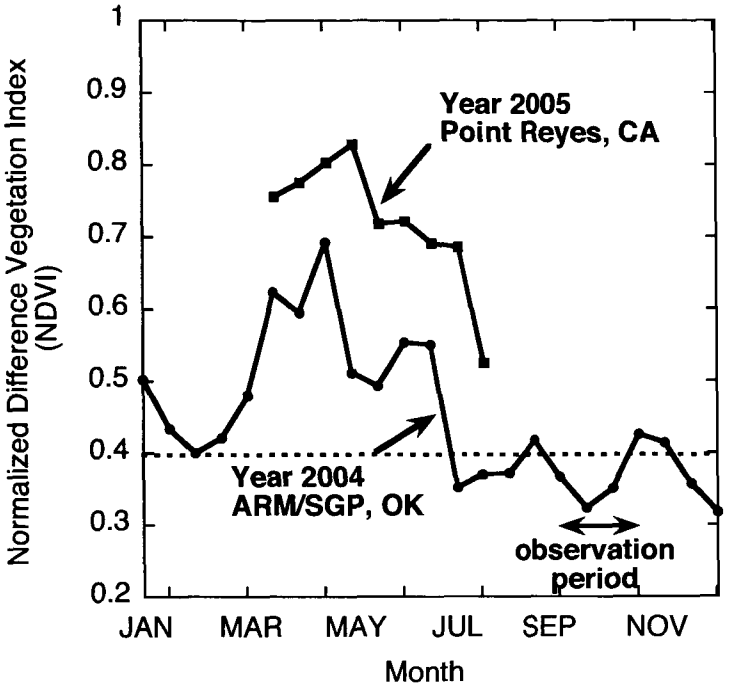

Fig. 6 Normalized difference vegetation index (NDVI) from MODIS for the ARM SGP site, 2004, and for Point Reyes, CA, 2005. The dashed line represents the threshold of 0.4. A NDVI smaller than this threshold often indicates an unsuitable surface reflectance contrast between RED and NIR channels.

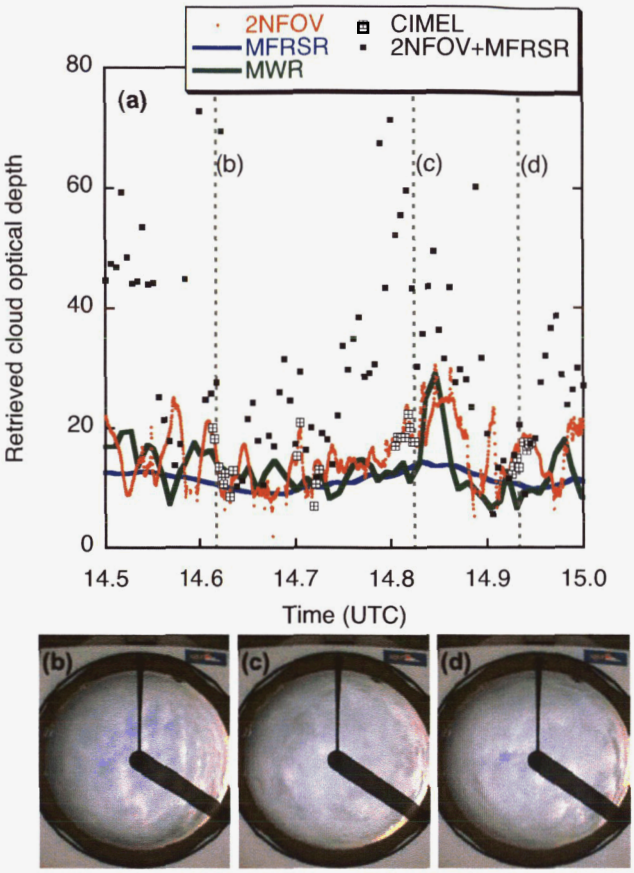

Fig. 7 (a) Retrieved cloud optical depths at the ARM SGP site for 14.5 to 15 UTC on Nov. 11, 2004. Solar zenith angles are between 70 and 75°. Surface albedo values are $\rho_{RED} = 0.17$ and $\rho_{NIR} = 0.36$. CIMEL observations were available for this day. TSI images were taken at (b) 14.62, (c) 14.83, and (d) 14.93 UTC. Red dots are retrievals based on 2NFOV-measured radiance and the RED vs. NIR algorithm. Blue lines are based on MFRSR-measured flux and an algorithm similar to Min and Harrison (1996). Green lines are based on MWR-retrieved liquid water path and an assumed 8μm droplet effective radius. Black squares are based on measurements of 2NFOV and MFRSR, and the COUPLED algorithm. CIMEL retrievals are obtained from the RED vs. NIR algorithm.

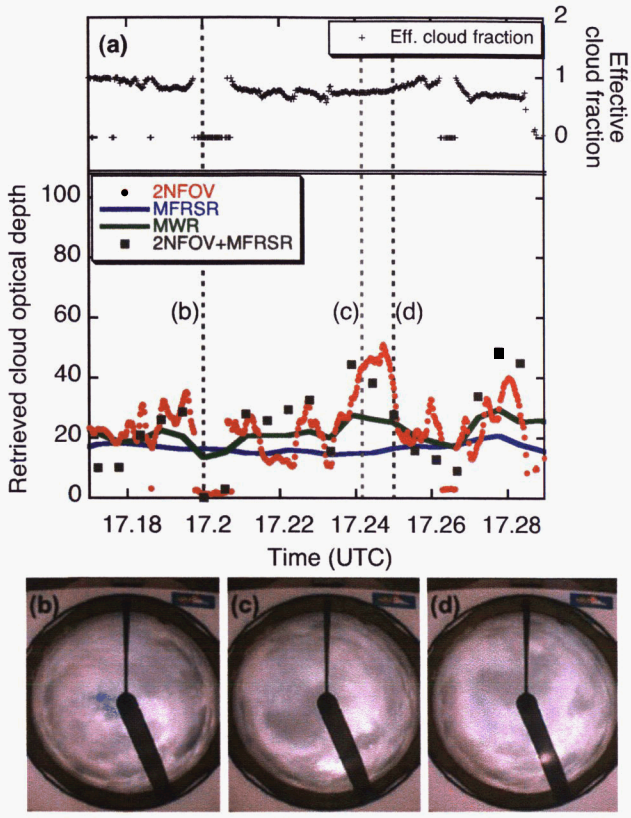

Fig. 8 (a) Same as Fig. 7, but for retrieved cloud optical depths (left y-axis) and effective cloud fractions (right y-axis) on Oct. 28, 2004. TSI snapshots are shown at (b) 17.20, (c) 17.24, and (d) 17.25 UTC. SZA = 52°. Surface albedo values are $\rho_{RED} = 0.13$ and $\rho_{NIR} = 0.28$.

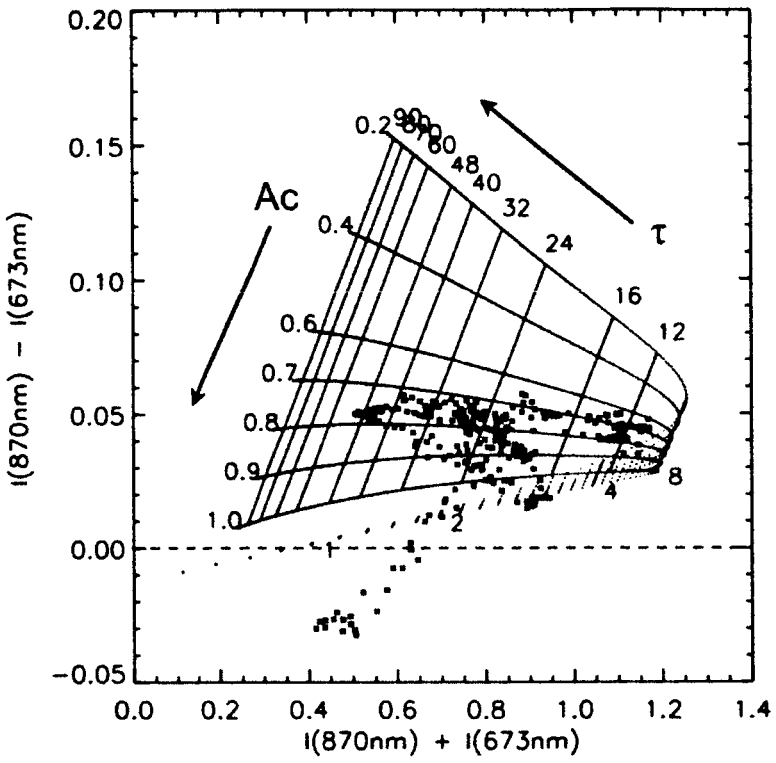

Fig. 9 A lookup table (lines) constructed for SZA = 52°; effective radius of 8 μm; and surface albedos of 0.13 and 0.28 for RED and NIR channels, respectively. The ARM 2NFOV measurements at the SGP site between 17.2 and 17.28 UTC, 2004/10/28 are illustrated by dots.

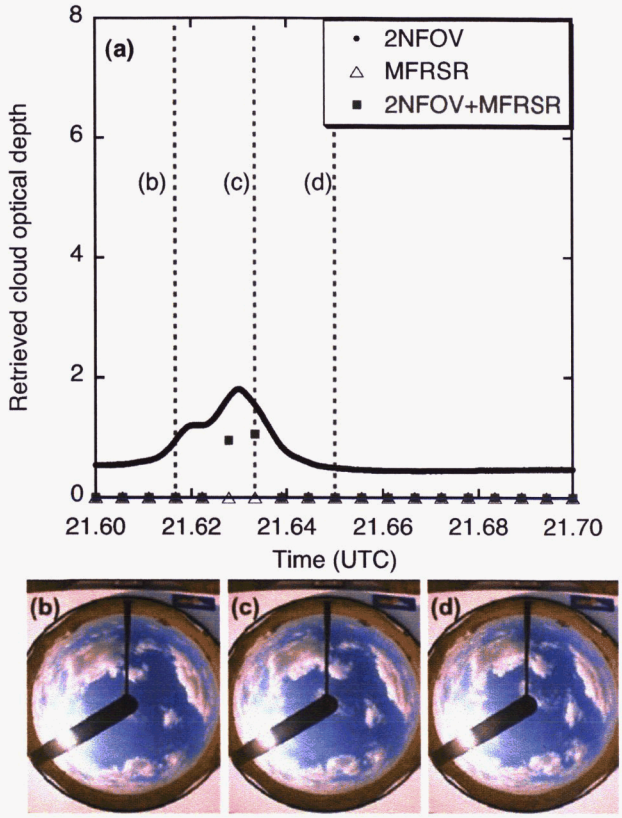

Fig. 10 (a) Same as Fig. 7(a), but for 21.6 – 21.7 UTC, Sep. 29, 2004. TSI images were taken at (b) 21.62, (c) 21.63, and (d) 21.65 UTC. $\rho_{RED} = 0.13$, $\rho_{NIR} = 0.28$, and SZA = 61°.

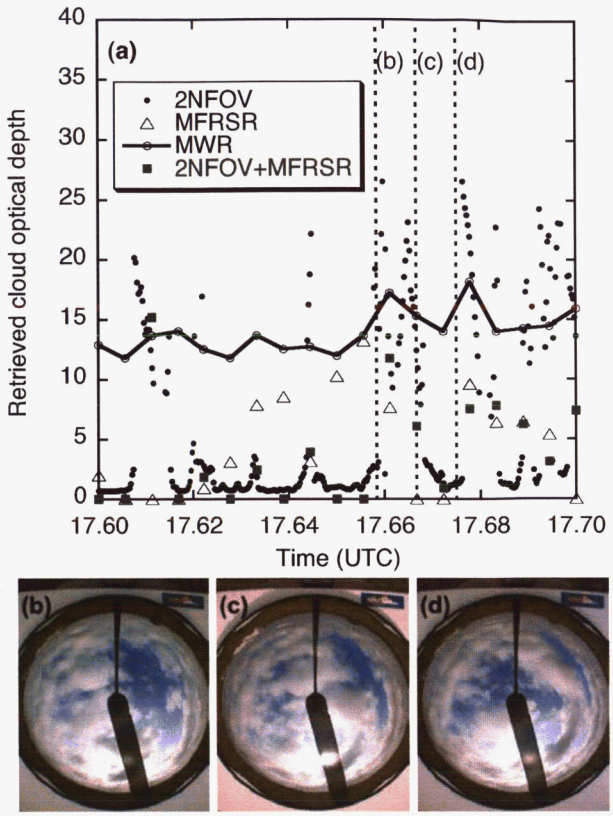

Fig. 11 (a) Same as Fig. 7(a), but for 17.6 – 17.7 UTC, Oct. 28, 2004. TSI images were taken at (b) 17.66, (c) 17.67, and (d) 17.68 UTC. $\rho_{RED} = 0.13$, $\rho_{NIR} = 0.28$, and SZA = 51°.

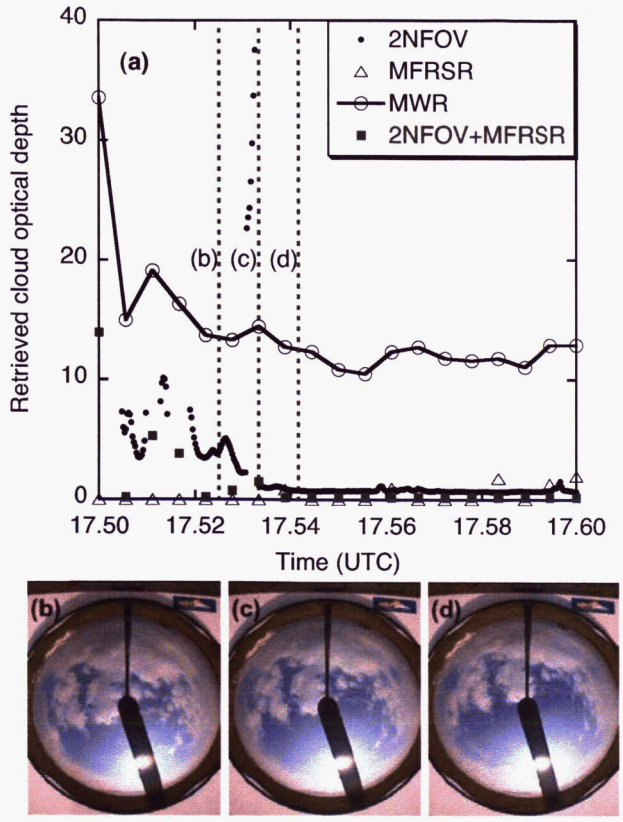

Fig. 12 (a) Same as Fig. 7(a), but for 17.5 – 17.6 UTC, Oct. 28, 2004. TSI images were taken at (b) 17.525, (c) 17.53, and (d) 17.54 UTC. $\rho_{RED} = 0.13$, $\rho_{NIR} = 0.28$, and SZA = 51°.

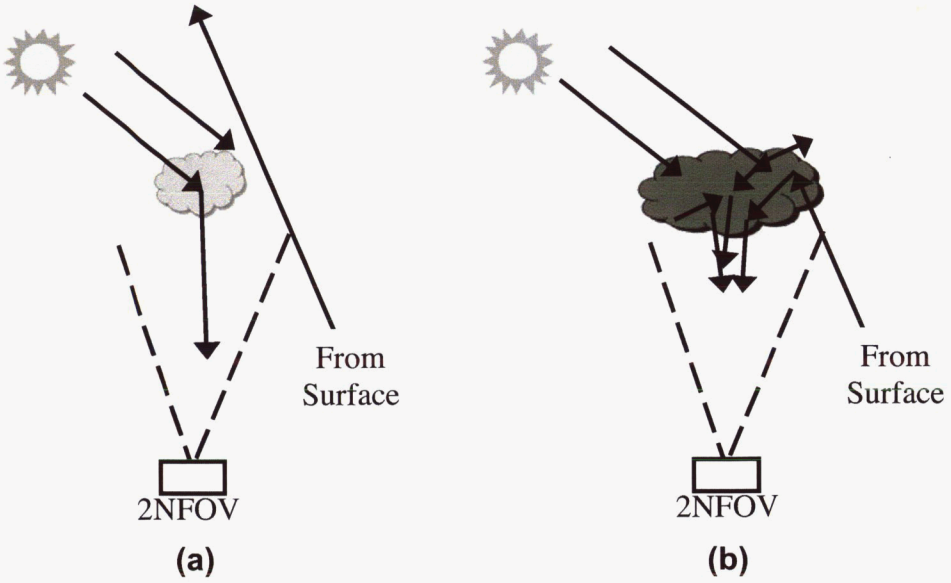

Fig. 13 Schematic illustration of radiances received by the 2NFOV radiometer for two cases: (a) the FOV is *partially* covered by thin clouds; and (b) the FOV is *fully* covered by thick clouds. In both cases the 2NFOV radiometer receives the same amount of radiation.

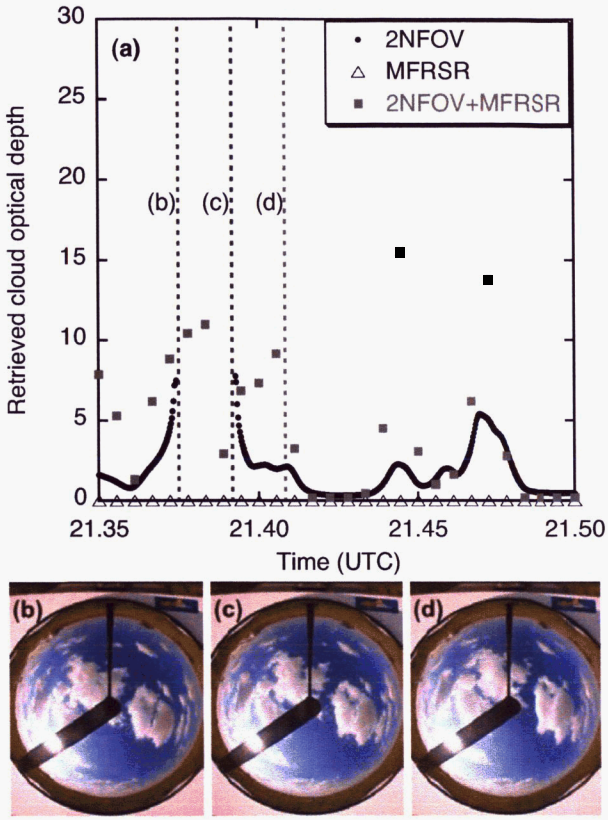

Fig. 14 Same as Fig. 7, but for 21.35 – 21.50 UTC, Sep. 29, 2004. TSI snapshots were taken at (b) 21.375, (c) 21.39, and (d) 21.41 UTC. Surface albedo in this case is dependent on solar zenith angle. $\rho_{RED} = 0.13$, $\rho_{NIR} = 0.28$, and SZA = 58°±1.

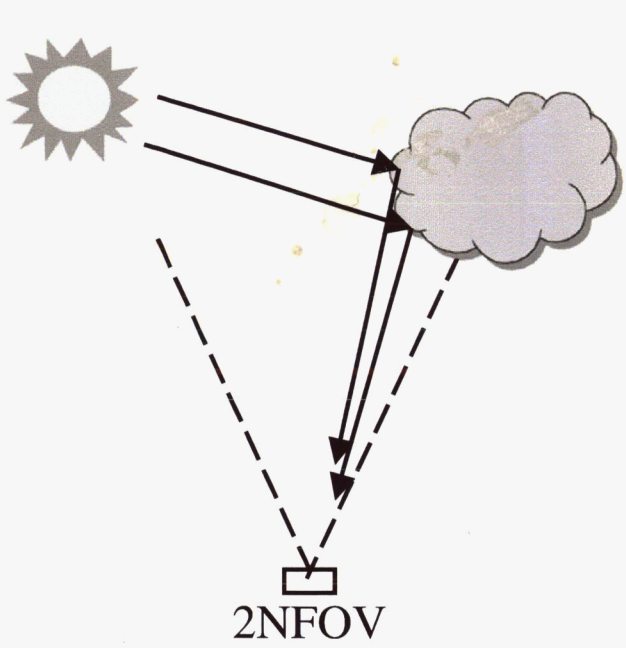

Fig. 15 Schematic illustration depicting a problematic situation for the RED vs. NIR algorithm in which cloud edges are illuminated by the Sun. This situation causes significant scattering of photons into the field-of-view of the radiometers. It leads to large radiances in both RED and NIR regions, which are outside of lookup tables and thus not retrievable.

Abstract

An extensive verification of cloud property retrievals has been conducted for two algorithms using zenith radiances measured by the Atmospheric Radiation Measurement (ARM) Program ground-based passive two-channel (673 and 870 nm) Narrow Field-Of-View Radiometer. The underlying principle of these algorithms is that clouds have nearly identical optical properties at these wavelengths, but corresponding spectral surface reflectances (for vegetated surfaces) differ significantly. The first algorithm, the RED vs. NIR, works for a fully three-dimensional cloud situation. It retrieves not only cloud optical depth, but also an effective radiative cloud fraction. Importantly, due to one-second time resolution of radiance measurements, we are able, for the first time, to capture detailed changes in cloud structure at the natural time scale of cloud evolution. The cloud optical depths τ retrieved by this algorithm are comparable to those inferred from both downward fluxes in overcast situations and microwave brightness temperatures for broken clouds. Moreover, it can retrieve τ for thin patchy clouds, where flux and microwave observations fail to detect them. The second algorithm, referred to as COUPLED, couples zenith radiances with simultaneous fluxes to infer τ. In general, the COUPLED and RED vs. NIR algorithms retrieve consistent values of τ. However, the COUPLED algorithm is more sensitive to the accuracies of measured radiance, flux, and surface reflectance than the RED vs. NIR algorithm. This is especially true for thick overcast clouds where it may substantially overestimate τ.

Chiu, J. C. and A. Marshak, Y. Knyazikhin, W. Wiscombe, H. Barker, J. C. Barnard, and Y. Luo

Remote sensing of cloud properties using measurements of zenith radiance

submitted to *J. Geophys. Res.*

Popular Summary

An extensive verification of cloud property retrievals has been conducted for two algorithms using zenith radiances measured by the Atmospheric Radiation Measurement (ARM) Program ground-based passive two-channel (673 and 870 nm) Narrow Field-Of-View Radiometer. The underlying principle of these algorithms is that clouds have nearly identical optical properties at these wavelengths, but corresponding spectral surface reflectances (for vegetated surfaces) differ significantly. The first algorithm, the RED vs. NIR, works for a fully three-dimensional cloud situation. It retrieves not only cloud optical depth, but also an effective radiative cloud fraction. Importantly, due to one-second time resolution of radiance measurements, we are able, for the first time, to capture detailed changes in cloud structure at the natural time scale of cloud evolution. The cloud optical depths τ retrieved by this algorithm are comparable to those inferred from both downward fluxes in overcast situations and microwave brightness temperatures for broken clouds. Moreover, it can retrieve τ for thin patchy clouds, where flux and microwave observations fail to detect them. The second algorithm, referred to as COUPLED, couples zenith radiances with simultaneous fluxes to infer τ. In general, the COUPLED and RED vs. NIR algorithms retrieve consistent values of τ. However, the COUPLED algorithm is more sensitive to the accuracies of measured radiance, flux, and surface reflectance than the RED vs. NIR algorithm. This is especially true for thick overcast clouds where it may substantially overestimate τ.